Peculiar magnetic states in the double perovskite Nd_{2}NiMnO_{6}

Somnath Pal, Somnath Jana, Sharada Govinda, Banabir Pal, Sumanta Mukherjee, Samara Keshavarz, Danny Thonig, Yaroslav Kvashnin, Manuel Pereiro, Roland Mathieu, Per Nordblad, John W. Freeland, Olle Eriksson, Olof Karis, and D. D. Sarma

Phys. Rev. B **100**, 045122 — Published 16 July 2019

DOI: 10.1103/PhysRevB.100.045122

Curious magnetic states in double perovskite Nd_2NiMnO_6

Somnath Pal,[1] Somnath Jana,[2,*] Sharada Govinda,[1] Banabir Pal,[1] Sumanta Mukherjee,[1] Samara Keshavarz,[2] Danny Thonig,[2] Yaroslav Kvashnin,[2] Manuel Pereiro,[2] Roland Mathieu,[3] Per Nordblad,[3] John W. Freeland,[4] Olle Eriksson,[2,5] Olof Karis,[2] and D. D. Sarma[1,†]

[1]*Solid State and Structural Chemistry Unit, Indian Institute of Science, Bengaluru 560012, India*

[2]*Department of Physics and Astronomy, Uppsala University, Box 516, SE-75120 Uppsala, Sweden*

[3]*Department of Engineering Sciences, Uppsala University, Box 534, SE-751 21 Uppsala, Sweden*

[4]*Argonne National Laboratory, Argonne, Il 60439 , USA*

[5]*School of Science and Technology, Örebro University, SE-70182 Örebro, Sweden*

(Dated: June 22, 2019)

Abstract

We present magnetic measurements on Nd_2NiMnO_6 which exhibits a well-known insulating paramagnetic state to an insulating ferromagnetic state transition when cooled below 200 K. Beyond this basic fact, there is a great deal of diversity in the reported magnetic properties and interpretation of specific anomalies observed in the magnetic data of this compound below the Curie temperature. We address specifically two anomalies discussed in the past, namely a spin-glass like behaviour observed in some samples near 100 K and a downturn in the magnetization with a lowering of the temperature below approximately 50 K. We show for the first time that the application of an increasing magnetic field can systematically change the low temperature behaviour to make the down-turn in the magnetization into an upturn. With the help of first principle calculations and extensive simulations along with our experimental observations, we provide a microscopic understanding of all magnetic properties observed in this interesting system to point out that the glassiness around 100 K is absent in well-ordered samples and that the low temperature magnetic anomaly below 50 K is a consequence of a ferromagnetic coupling of the Nd spin-moments with the spin of the Ni-Mn ordered sublattice without giving rise to any ordering of the Nd sub-lattice that remains paramagnetic, contrary to earlier claims. We explain this counter-intuitive interpretation of a ferromagnetic coupling of Nd spins with Ni-Mn spin giving rise to a decrease in the total magnetic moment by noting the less than half-filled $4f$ occupation of Nd that ensures orbital and spin moments of Nd to be opposite to each other due to the spin-orbit coupling. Since the ground state total magnetic moment of Nd has a contribution from the orbital moment, that is larger than the spin moment, the total moment of Nd is indeed pointing in a direction opposite to the direction of spin moments of the Ni-Mn sublattice as a consequence of the ferromagnetic exchange coupling between Nd and Ni-Mn spins.

I. INTRODUCTION

A versatile and promising class of magnetic materials is double perovskites with a general formula of $A_2BB'O_6$, with an ordered arrangement of corner-sharing BO_6 and $B'O_6$ units alternating in the crystal structure[1–4]. This and related classes of oxides allow a large variety of physical properties, in particular electric and magnetic ordering with suitable choices of metal ions at the A, B, and B' sites. Among such materials, La_2NiMnO_6, with A=La, B=Ni, and B'=Mn, has attracted a great deal of interest due to its rich physics, particularly large dielectric anomalies, magneto-capacitance effect and strong coupling between the magnetic, phononic and electronic degrees of freedom. It is a ferromagnet near room temperature with a Curie temperature of 280 K,[3–11] caused by the dominant Ni^{2+}–O^{2-}–Mn^{4+} ferromagnetic super-exchange coupling of the ordered structure. Further, a remarkable spin-glass state was found at 70 K due to the anti-site disorder between Ni^{2+} and Mn^{4+} ions that leads to Mn^{4+}–O^{2-}–Mn^{4+} and Ni^{2+}–O^{2-}–Ni^{2+} antiferromagnetic couplings.

A clear understanding of the electronic couplings, the distortion in the Ni^{2+}-O^{2-}-Mn^{4+} bond and their impact on the magnetic ordering is of great importance, in particular, to design different multifunctional materials of a similar kind. These controlling parameters can be tuned by changing the rare-earth ion at the A-site with the general formula A_2NiMnO_6. For example, double perovskites with A = Nd and Y exhibit monoclinic $P2_1/n$ phase, where, on the other hand, other rare-earth ions at the A-site lead to the rhombohedral ($R\bar{3}$) structure with a partial ordering of Ni and Mn atoms. It has been reported[3,4,12–16] that mixed valence states of the Ni and Mn can cause different structures, however, a final experimental evidence on the mechanism for the different structures is still missing[4,17]. Moreover, from the viewpoint of magnetism, it is interesting to probe the consequence of replacing the nonmagnetic La ion with a magnetic one, such as Nd in La_2NiMnO_6, since the magnetic interaction of the magnetic rare-earth ion with the Ni-Mn sublattice brings in another energy scale into the problem, thereby, promising a richer phase diagram.

Previous experiments[18–22] indeed suggest a richer magnetic behaviour for Nd_2NiMnO_6. All past publications agree on the existence of a clear ferromagnetic ordering of the Ni-Mn sublattice at about 200 K. This ordering temperature is somewhat lower than the corresponding value (260 K) in La_2NiMnO_6 due to a smaller Ni-O-Mn bond angle in the Nd compound[18], leading to a reduction of the ferromagnetic super-exchange interaction[3] re-

sponsible for the ferromagnetic state. Interestingly, magnetic properties of Nd_2NiMnO_6 below this temperature differ significantly between different reports. For example, there are reports[19,21] of a second magnetic transition around 100 K. This was explained[19] in terms of a different magnetic phase arising from different valence states, Ni^{3+} and Mn^{3+}, instead of the usual Ni^{2+} and Mn^{4+} responsible for the 200 K transition. Another report[21] pointed to the additional possibility of anti-site defects leading to antiferromagnetic interactions and consequent magnetic frustrations in analogy to the case of La_2NiMnO_6,[4] showing distinct signatures of glassiness and associating it with a cluster-glass behaviour. It is to be noted that these features near the 100 K are not reported in all studies of Nd_2NiMnO_6. However, there is again a general agreement on the observation of a downturn of the magnetization with a decreasing temperature at about 50 K which is deep within the ferromagnetic state,[18–22] though there is no clear consensus on the nature of this downturn in the magnetization. On the basis of neutron diffraction studies, it has been suggested[22] to be yet another magnetic transition where the Nd moments order ferromagnetically within a sublattice that is antiferromagnetically oriented with respect to the Ni-Mn ferromagnetically coupled sublattice. On the other hand, high temperature susceptibility has been shown[18] to be consistent with Nd ions being noninteracting and giving rise to a purely Curie, as against Curie-Weiss, behaviour; this would argue against any magnetic ordering of the Nd sublattice at a relatively high temperature of 50 K. Within such a noninteracting scenario, the downturn in the magnetization with decreasing temperature was tentatively interpreted as a manifestation of a "large magnetocrystalline anisotropy due to spin-orbit coupling of the Mn-Ni network to the rare earth" in Ref. 18. While the same interpretation of the downturn in $M-T$ was repeated in Ref. 19, this part of the magnetic behaviour was within what was attributed to the cluster glass state of Nd_2NiMnO_6 in Ref. 21.

With these controversies and the richness of magnetic properties in mind, we synthesized and investigated magnetic properties of Nd_2NiMnO_6, combining DC and AC magnetic investigations as well as magnetic spectroscopic study, in conjunction with detailed first principle calculations to provide a microscopic description of its magnetic interactions and states. Our results clearly show that Nd_2NiMnO_6 contains only Ni^{2+} and Mn^{4+} species with no perceptible signature of Ni^{3+} or Mn^{3+}. Like every other report, our magnetic measurements also confirm a magnetic ordering at about 200 K. X-ray magnetic circular dichroism measurements confirm the ferromagnetic coupling of the Ni and Mn sublattices below this ordering

temperature. Our magnetic measurements do not reflect any magnetic anomaly around 100 K, unlike Refs. 19, 21, but consistent with Refs. 18, 20, 22, presumably due to a lower number of anti-site defects, necessary to induce sufficient frustrations in magnetic interactions[4]. Accordingly, our AC magnetic measurements also do not indicate any glassy state at any temperature unlike Ref. 21. Our main results relate to the curious downturn in the $M(T)$ below about 50 K, reported by all studies[18–23] and interpreted often as an indication of the ordering of the Nd moments, coupled antiferromagnetically to the ordered Ni-Mn sublattice. Based on applied magnetic field and frequency dependencies of the magnetization over the relevant range of temperatures, we show that this cannot be associated with a second magnetic phase transition, associated with a spontaneous, long-range ordering of moments on the Nd-sublattice. Instead, it is to be understood in terms of a continuously increasing orientational ordering of the Nd moments due to the decreasing temperature in presence of the internal exchange field exerted by the ordered Ni-Mn sublattice. Our detailed, first principles electronic structure calculations help us to estimate the microscopic exchange interaction strengths between different ions, establishing that the spin-spin interaction between all nearest neighbour pairs, namely Ni-Mn, Nd-Ni and Nd-Mn, are ferromagnetic in nature, apparently in contradiction with the presumed antiferromagnetic coupling of Nd moments to the moment of the Ni-Mn sublattice and driving the downturn in $M(T)$ below about 50 K. We show that this counterintuitive downturn in $M(T)$ can be rationalized on the basis of the spin-orbit coupling within the Nd $4f$ manifold; these conclusions are supported by our detailed simulation of magnetization dynamics including the orbital moment on Nd, providing a microscopic understanding of the curious magnetization behavior of Nd_2NiMnO_6 at lower temperatures. We note that our findings do not contradict earlier reports on $Nd_xCa_{1-x}FeMoO_6$[24,25], where the change in magnetization is attributed to a band filling effect and increased anti-site disorder with increasing Nd doping, and consequently not resulting in any of the magnetic phenomena observed by us for Nd_2NiMnO_6.

II. EXPERIMENTAL AND THEORETICAL METHODS

A. Experimental

A pure monoclinic crystallographic phase of Nd_2NiMnO_6 was prepared by sol-gel method[17,18]. Nd_2O_3, $Ni(NO_3)_2$, $6H_2O$ and $MnCO_3$ were dissolved in stoichiometric quantities using dilute nitric acid. Subsequently, Ethylene Glycol and Citric acid were added to the solution as chelating agents for the gel formation. The gel was heated at 170 °C to get rid of the solvent completely. The obtained black colored powder was then heated at 450 °C for 6 hours to ensure decarboxylation. Following the decarboxylation step, the powder was pressed into a pellet and sintered at 1350 °C for 6 hours in the presence of flowing Argon gas for the final sample.

Powder X-ray diffraction (XRD) was collected using a Philips X′-Pert Diffractometer (Ni filtered Cu K_α radiation (λ = 1.54056 Å)). X-ray absorption spectroscopy (XAS) and X-ray magnetic circular dichroism (XMCD) measurements at Nd $M_{4,5}$, Ni $L_{2,3}$ and Mn $L_{2,3}$ edges were performed at the synchrotron light source, Maxlab, Sweden and the Advanced Photon Source, USA, respectively. The data were recorded using the total electron yield method by recording the sample drain current as a function of the photon energy. The base pressure of the chamber was maintained at around 3×10^{-10} mbar. Clean sample surfaces were exposed for experiments by scraping the sample surfaces in-situ with a diamond file. Magnetic measurements were performed by using a SQUID magnetometer from Quantum Design, USA.

B. First-principles calculations

For the electronic structure calculations reported in this work, the monoclinic crystal structure of Nd_2NiMnO_6 with the space group of $P2_1/n$ has been used, with the lattice parameters of a = 5.41 Å, b = 5.46 Å and c = 7.67 Å obtained from experiments. The k integration over the Brillouin zone is carried out using $12 \times 12 \times 8$ points and the exchange-correlation interactions are described within the local spin density approximation (LSDA)[26].

In order to improve the treatment of the localized $3d$ electrons of Ni and Mn atoms, the static correction using the Hubbard U term is added to the LSDA Hamiltonian, referred as LSDA+U method[27]. The value of Hubbard U for $3d$ elements in different compounds

depends strongly on the screening and can vary in the range between 2 to 9 eV. Hund's exchange J_H is less material-dependent and usually takes the value of about 1 eV. In this work, we used U and J_H to be equal to 4 eV and 0.9 eV, respectively, for both Ni and Mn atoms, slightly larger than the values chosen in Ref. 28 for the effective Coulomb potential. However, the $4f$ electrons in Nd behave like atomic states, therefore the conventional DFT($+U$) fails to properly describe the strong electron correlations in this element[29]. One way to solve this problem, is to assume that the $4f$ electrons do not hybridize with the valence electrons and therefore treat the $4f$ electrons as spin-polarized core states. However, since the lanthanides show different valence states in different compounds (divalent $f^{n+1}[spd]^2$ or trivalent $f^n[spd]^3$), one should be careful with the choice of the occupation of the f orbitals. Nd has been shown to be trivalent in solids[30]. Therefore, we consider a valence of $f^3[spd]^3$ for this element treating the three $4f$ electrons as core states. The spin-moment was selected according to LS-coupling, i.e. 2 $(g_J - 1)$J, where J is 9/2 and g_J is the Landé g-factor. This means that the spin-moment of the three core-like 4f electrons was constrained in the calculations to follow Russel-Saunders coupling and to be consistent with the Standard-Model of the rare-earths[31]. Using this knowledge, the electronic structure as well as the magnetic ground state configuration of the system are investigated in the framework of the full-potential linear muffin-tin orbital (FP-LMTO) code RSPt[32], in the scalar relativistic approximation.

The converged electronic structure calculations were then used to calculate the interatomic exchange parameters. This is achieved by mapping the magnetic excitations onto the Heisenberg Hamiltonian:

$$\hat{H} = -\sum_{<i,j>} J_{ij} \boldsymbol{e}_i \cdot \boldsymbol{e}_j, \tag{1}$$

where J_{ij} is an exchange interaction between the two spins, located at sites i and j, and $\boldsymbol{e}_i$ is a unit vector along the magnetization direction at the corresponding site. The effective interatomic exchange interaction between magnetic atoms, evaluated this way, ensures incorporating the effects of all other atoms in the system, as details of the total electronic structure enters the Greens functions used for these calculations. In this work, the pairwise exchange parameters were obtained by means of the magnetic force theorem[33,34]. The J_{ij}'s were computed between the $3d$ states of transition metals and $6s$, $6p$ and $5d$ states of

Nd, using a projection to the so called muffin-tin heads [35]. Note here that the interatomic exchange integrals are evaluated between dispersive valence band states, where the overlap between site centered basis functions is finite. The 4f moment of the rare-earth moment is locked via a large intra-atomic exchange to the spd-states of the rare-earth site,[36] producing an effective exchange interaction between the largest moments of the system, i.e. the 3d moment of Mn and Ni and the 4f moment of Nd. More specific details regarding the evaluation of the exchange parameters, especially with respect to the choice of the basis set can be found in Ref. 37.

The full-relativistic treatment of the Kohn-Sham problem in the FP-LMTO methods allow to obtain magnetocrystalline anisotropies K_i of the metal ions Mn and Ni from total energy difference (ΔE) for two different directions of the magnetization, e.g., along (001) and (100). This methodology is however not applicable for rare-earths, if their $4f$ electrons are treated as core states. This is so, because the $4f$ crystal fields, necessary for the proper description of K_i's, are simply missing in such a calculation. Based on this knowledge, we obtained a total energy difference of $\Delta E = 0.2$ meV favoring (100) as the easy axis. We associate this energy to the anisotropy rising from Ni orbital moment. The reason for assigning the anisotropy to the Ni atom is that the obtained orbital moments for Ni ions are 0.16 μ_B and 0.19 μ_B along (001) and (100) directions, respectively, while for Mn ions this value is about 0.02 μ_B for both magnetization directions. According to Bruno's model, the difference between the orbital moments along the easy and hard directions is proportional to the magnetocrystalline anisotropy[38]. Therefore, the anisotropy of each Ni atom is considered 0.1 meV while for Mn it is set to 0. For the Nd atoms an *ad hoc* value of 0.1 meV is used here, similar to Ni.

The sets of $\{J_{ij}\}$ and $\{K_i\}$ are then used in Monte Carlo (MC) simulations of the classical Heisenberg model described by Eq. (1) at temperature T and external magnetic field $\boldsymbol{B}$. To estimate the Curie temperatures, we used the fourth-order size-dependent Binder cumulant[39], which is defined as

$$U_L = 1 - \frac{\langle M^4 \rangle_L}{2\langle M^2 \rangle_L^2}, \tag{2}$$

where M is the total or average magnetization. The symbol $\langle \ldots \rangle$ in the above equation represents the ensemble and time average. Binder cumulants exploit the critical point and

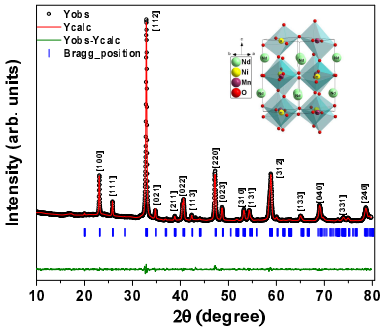

FIG. 1. (Colour Online) Observed (open circle), calculated (black line) and residual (green line) XRD pattern. Vertical lines are the Bragg peak positions.

critical exponents in a phase transition from the crossing point of magnetization curves for different sizes L of the system.

We performed Monte Carlo simulations by using the Uppsala atomistic spin dynamics (*UPPASD*) software[40] for systems with size ranging from $20 \times 20 \times 20$ (8000 atoms) up to $32 \times 32 \times 32$ (32768 atoms) employing periodic boundary conditions and $15 - 30$ replica of this system for a proper average of the properties. To perform hysteresis simulations at finite temperature, we effectively cooled down our system to certain T at very strong fields (field cooling). By doing this we achieve a ground state preferably aligned along the field. Without further field cooling, the external magnetic field is varied from -40 T up to 40 T.

III. RESULTS AND DISCUSSION

Powder XRD data of Nd_2NiMnO_6 is shown in Fig. 1. Rietveld refinement was performed using FULLPROF software, confirming the phase purity of our sample. Specifically, NiO, reported[19] as an impurity phase in samples of Nd_2NiMnO_6, is absent in our sample. XRD data could be fitted well with the crystallographic space group $P2_1/n$. The obtained lattice parameters a= 5.4142(1) Å, b = 5.4633(1) Å, c = 7.6690(1) Å; and β = 90.0207(1) are consistent with previous reports[18–21]. The unit cell of the ordered Nd_2NiMnO_6 is shown in the inset of Fig. 1 with alternating Ni and Mn atoms octahedrally coordinated by six oxygen atoms.

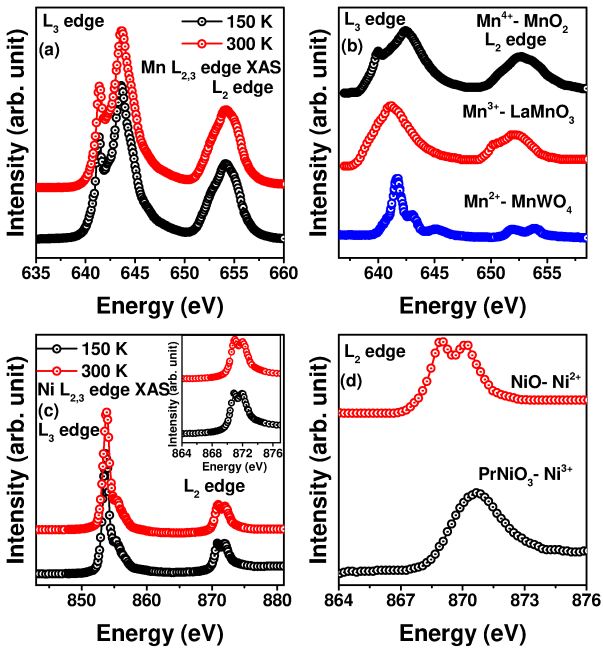

FIG. 2. (Colour Online) (a) Mn $L_{2,3}$ edge XAS spectra collected at 150 K and 300 K. (b) The characteristic XAS spectral of standard Mn-oxides samples, MnO_2, $LaMnO_3$ and $MnWO_4$ corresponding to Mn^{4+}, Mn^{3+} and Mn^{2+}, respectively. The spectrum of $MnWO_4$ is taken from Ref. 45. (c) Ni $L_{2,3}$ edge XAS spectra collected at 150°C and 300°C. (d) The characteristic XAS spectral of standard Ni-oxides samples, NiO and $PrNiO_3$ corresponding to Ni^{2+} and Ni^{3+}, respectively. The data for these two spectra of NiO and $PrNiO_3$ are taken from Ref. 4.

In Nd_2NiMnO_6, Nd and O are expected to be in their stable oxidation states, namely +3 and -2, respectively, while the valency of Mn and Ni may vary depending on their relative energy positions as well as on the hybridization and charge transfer energies[4,6,41]. A prior knowledge of the valencies of Mn and Ni is crucial to understand the magnetic properties of this sample. To this end, we have utilized the x-ray absorption spectra (XAS) at the Mn $L_{2,3}$ and Ni $L_{2,3}$ edges of Nd_2NiMnO_6, as this technique is a sensitive local probe to study the valence[42], spin character[43,44] and crystal field (CF) environment of different elements of a compound.

Fig. 2 (a) and (b) display the photon flux-normalized Mn $L_{2,3}$ spectrum from Nd_2NiMnO_6 at two temperatures and from a few standard Mn oxides with Mn in different valence states, respectively. Similarly, Fig. 2 (c) and (d) display the photon flux-normalized Ni $L_{2,3}$ XAS spectra from the sample at those two temperatures and from a couple of standard oxides

of Ni with Ni in different valence states, respectively. In all these cases, each spectrum corresponds to the $2p^6 3d^n \rightarrow 2p^5 3d^{n+1}$ transition and consists of two groups of multiplets, namely, the L_3 ($h\nu \sim 642$ (853) eV for Mn (Ni)) and L_2 ($h\nu \sim 653$ (872) eV for Mn (Ni)) separated by the spin-orbit splitting of the 2p core level. The line shape of the $L_{2,3}$ XAS spectrum of the transition metal elements depends strongly on the multiplet structure of $3d$-$3d$ and $2p$-$3d$ Coulomb and exchange interactions, as well as the local crystal field effects and the hybridization with the O 2p ligands, thereby providing characteristic changes in spectral features with the valence state of the transition metal ion as evident in Fig. 2 (b) and (d).

The Mn $L_{2,3}$ XAS spectra of our Nd_2NiMnO_6 sample are similar to those measured on La_2NiMnO_6[4,6], and the features clearly suggest that Mn is in +4 oxidation state in Nd_2NiMnO_6 (compare spectral features of Mn $L_{2,3}$ of MnO_2 sample in Fig. 2 (b)). The Ni $L_{2,3}$ XAS spectra are shown in Fig. 2 (c) for two different temperatures, and inset shows the magnified L_2 edge spectra. The line shape of Ni L_2 edge is very similar to that of NiO rather than that of $PrNiO_3$ (see Fig. 2 (d)). Therefore, we further confirmed from the Ni $L_{2,3}$ XAS results that the oxidation states of Ni ions are +2, which is consistent with the observation of the Mn in +4 state, i.e., fulfilling the charge balance requirement.

Fig. 3 (a) shows the magnetization (M) vs temperature (T) plots measured with an applied field of 20 Oe under both zero field cooled (ZFC) and field cooled (FC) conditions. The $M(T)$ data show a clear ferromagnetic (FM) transition at ~ 200 K and a magnetic anomaly at around 50 K, where the FC magnetization starts to show a gradual downturn with further lowering of the temperature of the sample. While the high temperature transition is well established to be the FM ordering of Ni-Mn sublattice, there is no consensus yet about the broad feature observed at the lower temperature. The downturn is obviously an indication of some antiferromagnetic alignment of some of the moments, its microscopic origin has not been satisfactorily described so far. While neutron diffraction results[22] have been used to suggest a ferromagnetic ordering of the Nd sublattice, coupled antiferromagnetically with the ferromagnetic Ni-Mn sublattice, the nature of $M(T)$ plot in Fig. 3 (a) is not the sharp change in magnetization that one would expect from the presence of a true phase transition with a spontaneous long range magnetic ordering below the critical temperature; instead $M(T)$ shows a more gradual change with a lowering of T. This point of view is further supported by the data obtained from the a.c. susceptibility measurements, discussed below.

AC measurements were performed at two different frequencies (17 Hz, 170 Hz) of the a.c. field. Fig. 3 (b) shows real (χ') (inset) and the imaginary (χ'') component of the a.c. susceptibility in the temperature range of 2-300 K. The magnetic phase transition at $\sim$ 200 K driving a ferromagnetic long-range order in the Ni-Mn sublattice is clearly indicated by the typical sharp changes in both χ' and χ''. There is no such sharp change in these quantities at any other temperature shown in Fig. 3 (b), arguing against a second magnetic phase transition in this system at $\sim$ 50 K. Instead, we only notice faint features in the out-of-phase component of the ac susceptibility, around $\sim$ 50 K, (see insets of Fig. 3 (b)), suggesting the lack of any reentrant spin glass behavior observed *e.g.* in La_2NiMnO_6.[4,46]. We do not notice any perceivable frequency dispersion in this low temperature magnetic feature, indicating an absence of any glassiness in the magnetic phase.

We have performed magnetization (M) measurements as a function of the applied magnetic field (H) at different temperatures to find a rather unusual magnetic behavior that has not been discovered or appreciated so far. $M(H)$ plots for various temperatures below the ferromagnetic transition (200 K) are shown in Fig. 4(a). The data for the highest temperature shown in the figure, namely 100 K, exhibits the $M - H$ hysteresis loop expected from a soft ferromagnet with a small coercive field ($\sim$ 200 Oe) and a near saturation of the magnetization at about 4.0 μ_B/f.u. for higher applied fields. In a normal situation, a lowering of the temperature should lead to a more clear saturation of the magnetization along with the possibility of an increasing coercive field, but $M(H)$ plots shown for successively lower T in Fig. 4(a) exhibits a progressively enhanced non-saturation of M with H at higher fields. This magnetic behavior suggests a magnetic configuration where paramagnetic Nd moments begin to be significantly influenced by coupling to the ferromagnetically ordered Ni-Mn sublattice well below its ferromagnetic transition temperature. An indication of the origin of this unexpected behavior is in the shape of the $M(H)$ curve for smaller values of H, where an enhanced coercivity is observed along the expected line. But along with that, the $M - H$ loop opens with an unusual shape, reminiscent of metamagnetic phenomena, suggesting that the applied magnetic field is responsible for influencing the magnetic state of the sample within this H and T ranges. Since the Ni-Mn sublattice orders ferromagnetically at a relatively high T of about 200 K, Ni-Mn sublattice at temperatures below 100 K is expected to be deep in the ferromagnetic state with little influence from the applied magnetic field. Thus, the only magnetic entity that can give rise to these unusual observa-

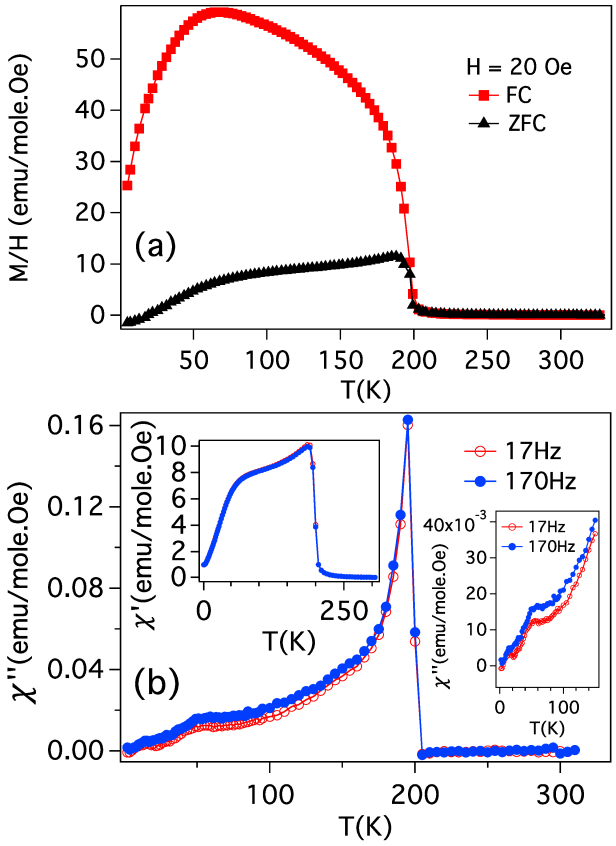

FIG. 3. (Colour Online) (a) The the filed cooled (FC) and zero filed cooled (ZFC) M/H, measured with an applied magnetic field (H) of 20 Oe. (b) The temperature variation of the imaginary part of the a.c. susceptibility at 17 Hz and 170 Hz with an amplitude of the a.c. field of 4.0 Oe. The two insets show the temperature variation of the real part of the a.c. susceptibility and an enlarged plot of the imaginary part of the a.c. susceptibility below 100 K in separate panels.

tions in $M(H)$ data is the magnetic moment of Nd^{3+} ion and its interaction with the Ni-Mn sublattice and the external, applied magnetic field.

If we combine our experimental results of $M(T)$ at low H in Fig. 3 (a) and of $M(H)$ at low T in Fig. 4(a), it presents an intriguing summary of magnetic behavior of Nd^{3+} ions - with a decreasing temperature, it increasingly aligns antiferromagnetically to the Ni-Mn sublattice, thereby reducing the total magnetization with decreasing T, while it increasingly aligns ferromagnetically to the Ni-Mn sublattice with an increasing H, showing an increasing trend in M. Thus, it appears that the effect of a decreasing T on Nd^{3+} ions can be opposed by an increasing H, since the two effects appear to influence it in a reversed manner. Thus, we investigated $M(T)$ in the low T regime for various values of the applied field, H and

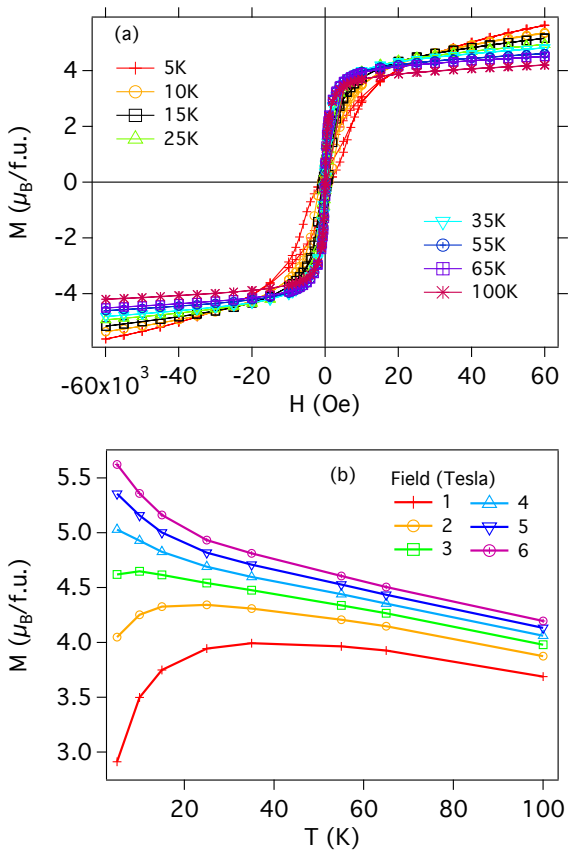

FIG. 4. (Colour Online) (a) Magnetization vs field loop measured at different temperatures. (b) Magnetization vs temperature measured at different applied field.

found the remarkable results, shown in 4(b), that the downturn in $M(T)$ for low H can be reversed into an upturn for $H > 3$ T, with $H = 3$ T being close to a compensation point.

While we shall discuss in detail implications of these unusual experimental observations later in conjunction with theoretical inputs, it is clear at a qualitative level that only the following scenario is consistent with all observations, described here so far. Moments on Nd ions tend to align antiferromagnetically with respect to the magnetization of the Ni-Mn sublattice, leading to the decrease in the sample magnetization with decreasing T for low applied fields; the continuously decreasing trend of the magnetization with T is a reflection of lowering of T that allows a progressive reduction in the thermal disordering of Nd moments rather than a spontaneous magnetization developing in the Nd sublattice due to a magnetic phase transition. With an increasing external magnetic field, moment on the Nd ions prefer to align with the applied field, overcoming the internal antiferromagnetic coupling with the

Ni-Mn sublattice. Thus, the existence of this compensation point at $H = 3$ T, not realised in the literature before, represents a balance between the internal antiferromagnetic coupling and the coupling to the external field of Nd moments, thereby allowing us to estimate several important quantities for this system. For example, it is evident that the compensating field of 3 T provides us with a reliable measure of the exchange interaction strength between the Nd^{3+} ion and the Mn-Ni magnetic sublattice. Since a moment of 1 μ_B in 1 T magnetic field has an energy of 5.8 x 10^{-2} meV, the compensating magnetic field of 3 T for the total magnetic moment (3.27 μ_B) of a Nd^{3+} ion represents about 0.6 meV as an estimate of the coupling of the Nd ions to the Ni-Mn sublattice. Moreover, at this compensated point, the magnetization follows the usual Bloch $T^{3/2}$ nature of a ferromagnetic sample with contribution from Nd moments essentially removed; therefore, we obtain a reliable estimate of the low T saturation moment of the Ni-Mn ferromagnetic sublattice as ~ 4.7 μ_B per f.u. (see Fig. 4(b)). This would suggest that there is a high degree ($\sim$ 97%) of Ni/Mn order, since the ideally ordered structure has a combined (Ni+Mn) moment of 5 μ_B per f.u. and each anti-site disordered Ni-Mn pair decreases the moment by 10 μ_B per pair. This low level of anti-site defect density ($\simeq$ 3%) in our sample is possibly responsible for avoiding the glassy physics observed[21] in some samples of Nd_2NiMnO_6. In order to obtain microscopic evidence into the nature of exchange couplings between different magnetic sites, namely Ni, Mn and Nd, in this sample, we have carried out detailed XMCD studies, since this is the only technique that can provide element selective magnetic information by tuning of the X-ray energy to the resonance absorption edges of specific elements. We discuss XMCD results obtained at Ni and Mn $L_{2,3}$ edges and Nd $M_{4,5}$ edges of our sample next.

Fig. 5 (a), (b), (c) show the XMCD spectra collected at Mn $L_{2,3}$, Ni $L_{2,3}$ and Nd $M_{4,5}$ edges, respectively, at 95 K. This temperature is chosen to be well below the high temperature magnetic transition at $\sim$200 K, but above the lower temperature ($\leqslant$ 50 K) region where the $M(T)$ shows a downturn with a decreasing temperature. Both Ni and Mn XMCD data (see Fig. 5 (a) and (b)) exhibit substantial intensity, clearly establishing the ferromagnetic nature of both Ni and Mn sublattices. We note that the sign of the leading edge of the XMCD signal with its relatively large weight (see Figs. 5 (a) and (b)) are given by the orientation of the spin moment contributed by that magnetic site. Therefore, the signs of the XMCD signals from Ni and Mn, with the leading edges being negative in both, indicate the same orientation of the spin moments on Ni and Mn sites, establishing the

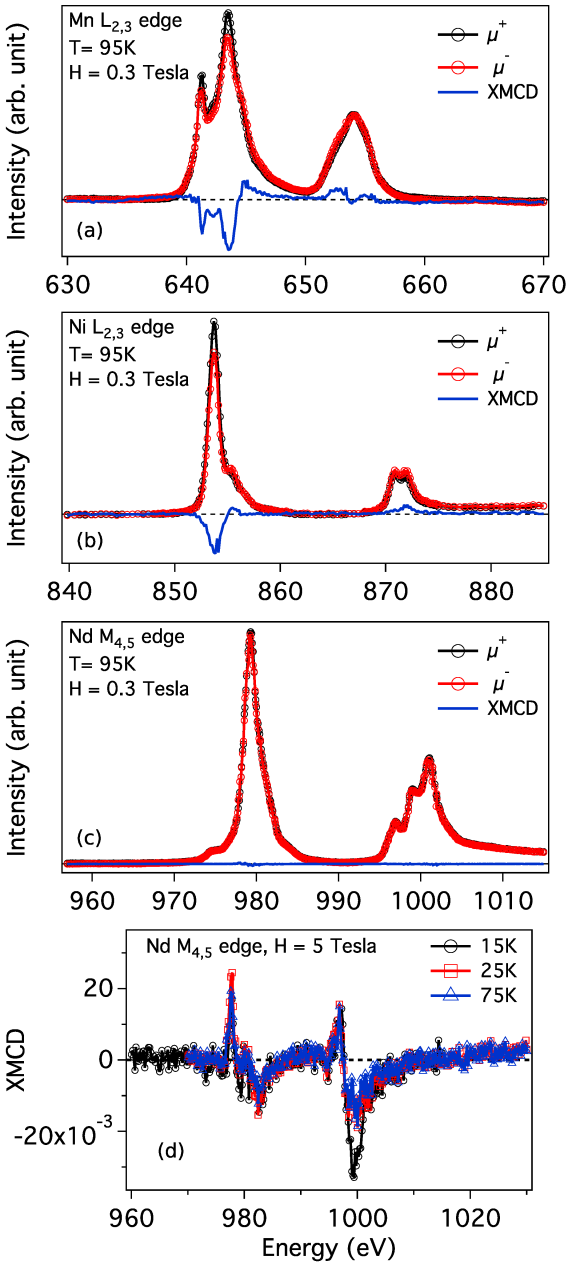

FIG. 5. (Colour Online) X-ray magnetic circular dichroism (XMCD) data collected over (a) Mn $L_{2,3}$ edge (b) Ni $L_{2,3}$ edge and (c) Nd $M_{4,5}$ edge at 95 K with an applied field of H= 0.3 T. (d) XMCD data collected over Nd $M_{4,5}$ edge at 15 K, 25 K and 75 K with an applied field of 5 Tesla.

ferromagnetic exchange coupling between Mn and Ni sublattices, leading to a ferromagnetic Ni-Mn sublattice below the phase transition temperature of ∼200 K, as also proposed in the case of La_2NiMnO_6[3]. In sharp contrast, there is no noticeable dichroic signal at the Nd edges, shown in Fig. 5 (c), recorded at the same temperature. It clearly suggests that

Nd moments are randomly oriented at this temperature, contributing no measurable net magnetization to the sample.

In order to see the origin of unusual magnetic properties observed below 50 K and at various magnetic fields, we recorded XMCD at Nd edges at 75 K, 25 K and 15 K, for a low field (0.3 T) and a high field of 5 T. We could not find any perceivable XMCD signal at the low field, suggesting the persistent paramagnetic nature of Nd ions at these low temperatures, arguing against any interpretation based on a spontaneous magnetization of the Nd sublattice with a long range magnetic ordering via a phase transition. At the high filed of 5 T, the paramagnetic moments on Nd ions are polarized by the external field, thereby giving rise to a measurable XMCD signal, shown in Fig. 5 (c). Interestingly, the leading edge of the XMCD signal from Nd at 5 T has the opposite sign compared to those at the Ni and Mn edges (see Figs. 5 (a) and (b)), indicating that the spin orientation of Nd moment is opposite of those of Ni and Mn. To the extent any magnetic moment would like to align itself with the external magnetic field in order to lower its energy, one would expect the spin moments of Ni-Mn ferromagnetic sublattice and that of the Nd sites would both be aligned with the applied field, thereby leading to a parallel arrangement of spins between Nd and Ni-Mn at this high field limit. The opposite result, observed here, can be understood by noting that the moment at the Nd site is not given only by the spin moment, but by the spin-orbit coupled total moment. Since Nd with its $4f^3$ configuration is less than half-filled, the ground state has the orbital and the spin moments oppositely aligned and the larger orbital moment dictates the orientation of the total moment. Therefore, the antiparallel orientation of the Nd spin moment with respect to the spin moment of Ni-Mn sublattice, in reality, ensures a parallel orientation of the total moment on the Nd site with that of the Ni-Mn sublattice, since dominant orbital moment of Nd is oriented in a direction opposite of that of its spin moment.

The above discussion, in conjunction with the magnetic data presented in Fig. 4(b) provides an interesting insight into the exchange coupling between Nd and Ni-Mn sublattice. XMCD data suggests that at 5 T applied field, the spin moment of Nd is antiparallel to Ni-Mn spin moments. Results in Fig. 4(b) showed that 5 T applied field is above the compensation point of 3 T and therefore, at 5 T, the spin orientation of Nd is opposite of what it will be at low fields of less than 3 T. This implies that the ground state exchange coupling between Nd and Ni and Mn sites must in fact be ferromagnetic, making the spin orientation at Nd, Ni

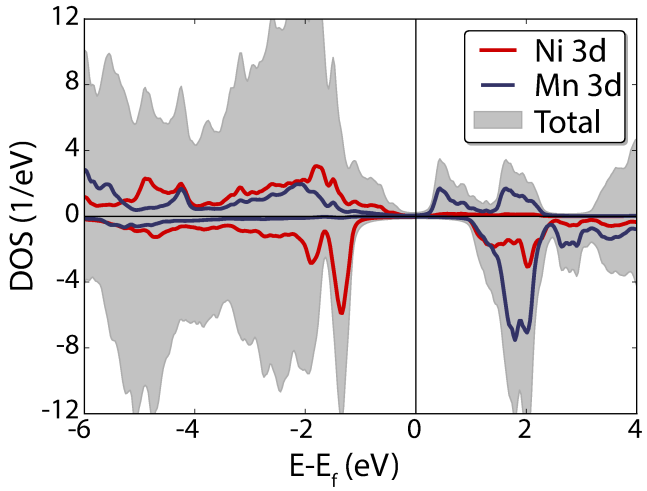

FIG. 6. (color online) Total density of states for majority and minority spin as well as the $3d$-projected density of Ni and Mn atoms in Nd_2NiMnO_6.

and Mn sites all being in the same direction. This view is consistent with the downturn in the magnetization with decreasing T (see Fig. 3 (a)), because the parallel orientation of the spin moment of Nd ensures an antiparallel orientation of the orbital moment which is larger than the spin moment. This interpretation provides a natural explanation for the unusual observation[18] of a similar downturn in the magnetization of Sm_2NiMnO_6 with a decreasing temperature whereas other Ln_2NiMnO_6 with Ln = Gd, Tb, Dy, and Ho exhibit an upturn; clearly, this is related to the less than hal-filled nature of Sm^{3+} in contrast to the half-filled or more than half-filled nature of the $4f$ orbitals in Gd, Tb, Dy, and Ho.

A. Ab-initio results

In order to give a firm footing to the above mentioned interpretation of magnetic properties of Nd_2NiMnO_6, we have performed first-principles calculations in order to get quantitative insights into the microscopic origin of various magnetic interactions.

In Fig. 6, the total density of state for the majority and minority spins as well as the total contribution of the d states of Ni and Mn atoms in the ground state are shown. A clear band gap of about 1 eV can be seen in the system, consistent with its insulating properties. The ground state of the system predicts parallel alignment of the Mn and Ni spin moments, with 2.87 μ_B for Mn and 1.49 μ_B for Ni ions. The total moment of Nd is, however, anti-parallel

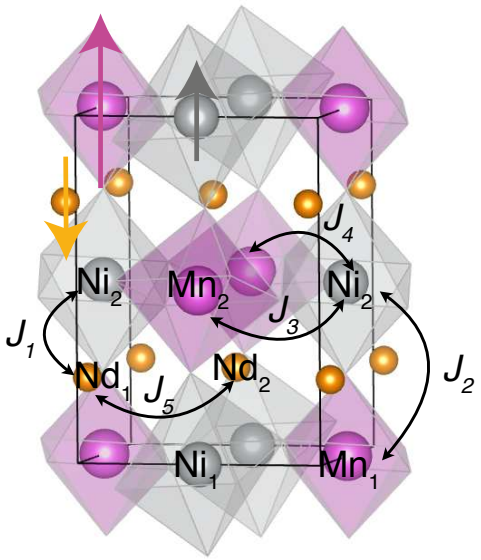

FIG. 7. (color online) The crystal structure of Nd_2NiMnO_6. The labels indicate the exchange couplings between, as an example, Ni_2 and the other atoms in the system. The exchange parameters between atom Ni, Mn, Nd with the neighbouring atoms in meV are as following: J_1=0.03 (0.23) between Ni (Mn) and Nd, $J_2 = 5.99$, $J_3 = 4.90$, $J_4 = 19.05$ and $J_5 \leq 0.01$ (due to the distortion in the system and smallness of J_1 and J_5, the averaged values are given). For the further neighbors the exchange parameters quickly decay to almost zero. For more detail, see Table I. The orientations of magnetic moments, including the spin and orbital contributions, at different sites in the ground state are shown on three types atoms in the top left corner of the unit cell. For the Nd site, the spin moment is oriented in a direction opposite to that of the total moment or in other words, in a parallel orientation with the spin moments of Ni and Mn shown here.

to the moments of Ni and Mn. The Nd ion has a total moment of 3.6 μ_B, associated with the spin and orbital momenta contributions in the LS-coupling scheme. The spin moment of a rare-earth from such calculations is best evaluated via Landé factor and the total angular momentum J which, as was described in Sec. IIB, is about 2.44 μ_B.

Based on the obtained electronic structure, we have calculated the magnetic exchange parameters (see Fig. 7 for labelling of different exchange parameters). Considering, as an example, the ion labelled Ni_2 at site i, J_1 will be the couplings between Ni_2 and its the nearest neighbours (labelled Nd_1 and Nd_2). This has quite small contribution to the total exchange interaction of the system. J_2 corresponds to the coupling between, e.g., Ni_2 and the Mn_1 ions. Due to the distortion, Ni_2 ion has two types of Mn_2 neighbors with the same

distance but different Ni-O-Mn angle (147° and 158°). J_3 and J_4 represent the interactions with Mn_2 ions of the angels 147° and 158°, respectively. Clearly, the leading interaction is the *in-plane* J_4 interaction. Finally, J_5 labels the coupling between Nd ions of different sites (Nd_1 and Nd_2) and as expected it is very small, due the extreme localization of the $4f$ electrons in rare-earth elements. In Table I, a list of the exchange parameters for different directions is shown. Note that according to Eq. 1, only the value of individual spin moments are encoded to the J_{ij}'s parameters, not the total moment associated to the spin and orbital momenta. We find that the dominant exchange parameters between atom Ni, Mn, Nd with the neighbouring atoms (in meV) are as follows: J_1=0.03 (0.23) between Ni (Mn) and Nd, J_2=5.99, J_3=4.90, and J_4=19.05 between various Ni-Mn pairs and J_5 between nearest neighbor Nd-Nd sites $\leq$ 0.1. For the further neighbors the exchange parameters quickly decay to almost zero.

Note that the exchange parameters discussed in the paragraph above were calculated for the ground state magnetic structure, where all spin-moments are coupled ferromagnetically. The transferability of these parameters to handle spin-configurations that are not the ground state configuration is a natural question, and we note that this issue has been discussed in the past, e.g. in Refs. 47, 48 and 49. Ref. 49 is particularly relevant for the present study, since it also describes calculations of Heisenberg exchange interactions of a 3d transition metal oxide. In this work the influence of the oxygen atoms was discussed, with a specific discussion of the fact that a relatively large polarization of the O states can provide a strong configurational dependence of the exchange parameters between transition metal atoms. In the present investigation the hybridization induced moment on the O atoms of the ground state configuration is in the range 0.004-0.067 μ_B/atom, depending on the position of the O atom in the unit cell. For spin configurations with higher energies, e.g. canted or antiferromagnetic couplings, the hybridization induced O moments is expected to be even smaller. The renormalization procedure of the Heisenberg exchange interactions, suggested in Ref. 49, is relevant only for situations where the O moment is distinctly different between different configurations, which is not the situation in the presently investigated systems. Hence, one can expect high transferability of the exchange parameters evaluated at the ground state configuration of Nd_2NiMnO_6.

Within our convention, a positive value of the J_{ij} indicates a FM coupling between the atomic spin moments at the two sites involved, indicating all dominant exchange couplings,

$J_1 - J_4$ are ferromagnetic in nature. The dominant exchange interactions between Ni and Mn sites, $J_2 - J_4$, being all ferromagnetic, is consistent with the prominent ferromagnetic state of the Ni-Mn sublattice in this compound. Nd-Nd interaction strength (J_5) is found to be very small, consistent with our interpretation that the magnetic anomaly seen around 50 K cannot be associated with a spontaneous ordering of Nd spins. Finally, it is interesting to note that the exchange coupling (J_1) between Nd and Mn/Ni being ferromagnetic (data not shown), is consistent with our interpretation of experimental results that suggested the total (spin-orbit coupled) moment of Nd is antiferromagnetically aligned with the spin moment of the Ni-Mn sublattice, thereby reducing the magnetic moment of the sample with a decrease in the temperature at low applied fields. Noting that the total moment of Nd^{3+} ion is oriented opposite to its spin moment, it is clear the spin-spin exchange interaction between Nd and Ni-Mn sublattice being ferromagnetic, as calculated here, is the driving force for the total moment of Nd being opposite to that of the Ni-Mn sublattice in the low field limit. Thus, the calculated results provide a qualitative and microscopic understanding of the magnetic properties observed in this material.

We note in passing that the average values of J_1 (0.036 and 0.226 meV for Nd-Ni and Nd-Mn, respectively) would suggest a somewhat larger magnitude of the compensating field

TABLE I. Exchange parameters (J_{ij}) between Ni and Mn in meV for different directions. Note that according to Eq. 1, the value of the magnetic moment of each site is included in the definition of J's .

Ni−Mn		Ni−Ni		Mn−Mn	
R_{ij}	J_{ij}	R_{ij}	J_{ij}	R_{ij}	J_{ij}
$[0, 0, +0.5]$	5.99	$[-1, 0, 0]$	-0.95	$[0, -1, 0]$	-0.27
$[0, 0, -0.5]$	5.99	$[+1, 0, 0]$	-0.95	$[0, +1, 0]$	-0.27
$[-0.5, +0.5, 0]$	19.05	$[0, 0, -1]$	-2.04	$[0, 0, -1]$	0.01
$[-0.5, -0.5, 0]$	4.90	$[0, 0, +1]$	-2.04	$[0, 0, +1]$	0.01
$[+0.5, +0.5, 0]$	4.90	$[-1, -1, 0]$	-3.27	$[-1, -1, 0]$	0.25
$[+0.5, -0.5, 0]$	19.05	$[+1, +1, 0]$	-3.27	$[+1, +1, 0]$	0.25

compared to 3 T obtained experimentally. Noting that each Nd site is coordinated by 4 Ni and 4 Mn sites, the total coupling strength between the Nd spin moment and the Ni-Mn sublattice works out to be 1.04 meV, whereas the corresponding value estimated from experimentally obtained compensating field of 3T is about 0.6 meV. This mismatch is not unexpected, since the estimates of exchange interaction strengths can have sizable percentage inaccuracies for such weak coupling strengths.

B. Magnetism from an effective spin-Hamiltonian

The exchange interactions between the atomic magnetic moments dictate their thermal behaviour. For this reason we performed Monte Carlo simulations based on the Metropolis algorithm and the classical spin-Hamiltonian Eq. (1) and obtain the magnetic phase diagram. To do the simulations in a proper way, one has to take into account that the Nd moment is anti-parallel to the Mn and Ni moments. The spin component of the Nd moment couples ferromagnetically with the moments of Ni and Mn ions. However, the relatively big orbital moment of Nd aligns antiparallel to the spin one, following the third Hund's rule

Since the ferromagnetic coupling strength of a Nd ion with its six nearest neighbor Nd ions is relatively weak ($\approx$0.6 meV = 7 K) and is much smaller than the Nd-Mn or Nd-Ni interactions, the Nd sublattice magnetisation is very temperature dependent. It looses correlation to other Nd atoms already at below 5 K. The calculated M versus T plot (Fig. 8(a)) shows a clear downturn with decreasing temperature below about 50 K, caused by the antiferromagnetic coupling between moments on Nd and Ni/Mn atoms. This is in excellent agreement with the behavior of the experimental $M(T)$ plot (Fig. 3). Calculated results suggest that the correlation of Nd to other atoms (Ni and Mn) drops off beyond about 65 K, leaving the system in a state where ferromagnetic coupling between the $3d$ ions dominates the magnetic behavior. From Binder's cumulant we obtain a critical temperature of T_c = 203 K, which is slightly below the phase transition temperature indicated by the peak in the specific heat (inset of Fig. 8(a)), which appears at T_c = 210 K. The calculated critical temperature is in excellent agreement with the experimentally measured T_c, suggesting the reliability of the calculated exchange interaction strengths within the Ni-Mn sublatticce. To get a deeper insight into the magnetic behaviors, we looked at the evolution of element-specific moments as a function of the temperature for all three magnetic sites and the results

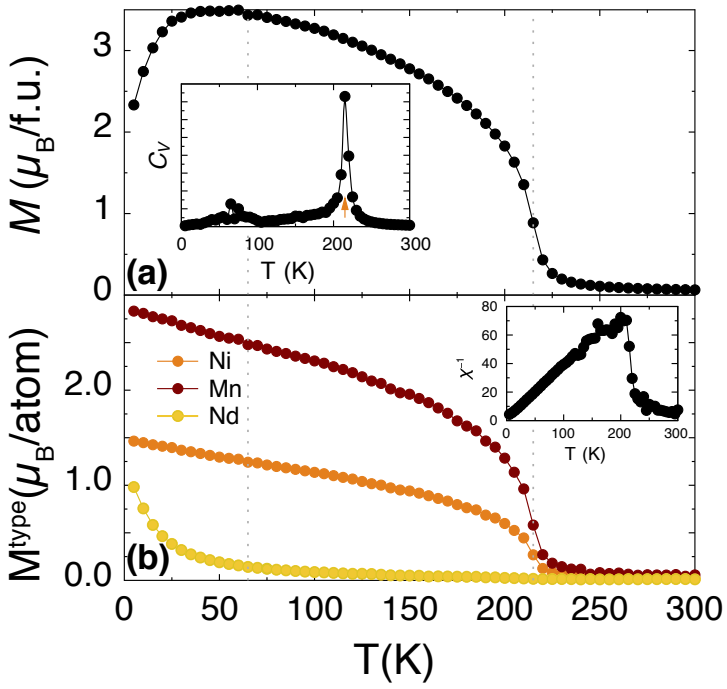

FIG. 8. (color online) (a) The total magnetization of Nd_2NiMnO_6 calculated as a function of temperature T. The inset shows the calculated specific heat as a function of temperature. The red arrow indicates the peak in C_V related to ferromagnetic phase transitions. (b) Element-specific magnetization calculated as a function of the temperature, where different elements are indicated by different colours. The inset shows the inverse susceptibility of Nd moments in presence of the internal field arising from ordered Ni+Mn moments (see text for more details) as a function of the temperature, suggesting a very close adherence to the Curie-like behavior.

are shown in Fig. 8(b). These plots clearly establish that Ni and Mn moments exhibit a typically ferromagnetic phase transition and have the same phase transition point at T_c with the spontaneous growth of magnetization at these two sites. Interestingly, the behavior of the calculated Nd moment is distinctly different from those of Ni and Mn, with the Nd moment smoothly varying in a way reminiscent of paramagnetic ions in an external magnetic field. In order to explore this description further, we have normalized the calculated Nd moment by the sum of Ni and Mn moments at each temperature point; then we have plotted the inverse of thus normalized Nd moment as a function of the temperature (inset to Fig. 8(b)). This normalized Nd moment can be viewed as the susceptibility of the Nd moment, where M_{Nd} is the magnetization of the Nd moment with the "applied magnetic field" on the Nd

moment being proportional to $(M_{Mn} + M_{Ni})$ that provides an internal field to align Nd moments. The inverse of this way extracted effective Nd susceptibility, plotted as a function of the temperature, shows a clearly nearly Curie Law, indicating that the Nd sublattice does not show any indication of any long range order at any temperature, but behaves only as individual paramagnetic moments in an internal field provided by the moments of Ni and Mn via the exchange coupling.

As already discussed, the total Nd moments are oriented in a direction opposite to those of Ni and Mn moments, giving rise to the downturn in the total moment with a decreasing temperature below about 50 K. We have also seen experimentally that it is possible to reorient and align the Nd total moments in the same direction as those of Ni and Mn by applying a large enough external magnetic field. It is interesting to estimate theoretically the magnitude of this external field required to turn around the Nd moments. Since the Heisenberg Hamiltonian (1) is isotropic and, thus, does not describe the hysteresis in the system, we have to extend the Hamiltonian (1) by adding the anisotropy term:

$$H_{anis} = \sum_i K_i \left(\boldsymbol{e}_i \cdot \boldsymbol{a}\right)^2 \tag{3}$$

with the easy axis along $\boldsymbol{a}$ and the atom-specific magnetocrystalline anisotropy constant K_i. From relativistic total energy simulations as described in Section II, we found negligible magnetocrystalline anisotropy for the Mn atoms, while an in-plane magnetization for Ni atoms with $K = 0.1$ meV. The anisotropy for Nd was chosen as a parameter in the simulations, which was fixed to $K = 0.1$ meV. Our external field was applied along the easy axis (z-direction). Taking into account H_{anis}, we performed a series of simulations of the system under different external fields to capture the spin reorientation of Nd moments.

Fig. 9 shows the theoretical values of magnetisation versus temperature, for various external field strengths. It can be seen that without an external field the M vs T curve has a decreasing trend below 65K, which represents a compensation point where the Nd and Mn and Ni moment cancel each other out. An applied field changes this picture, as Fig. 9 shows, since the Zeeman term starts to rotate the Nd moment to become gradually more and more parallel to the Mn and Ni moments. Hence, the possibility for a compensated sample disappears as the strength of the applied field increases, which is consistent with our experimental observations. However, it requires a relatively large field (≈30 T) to align all

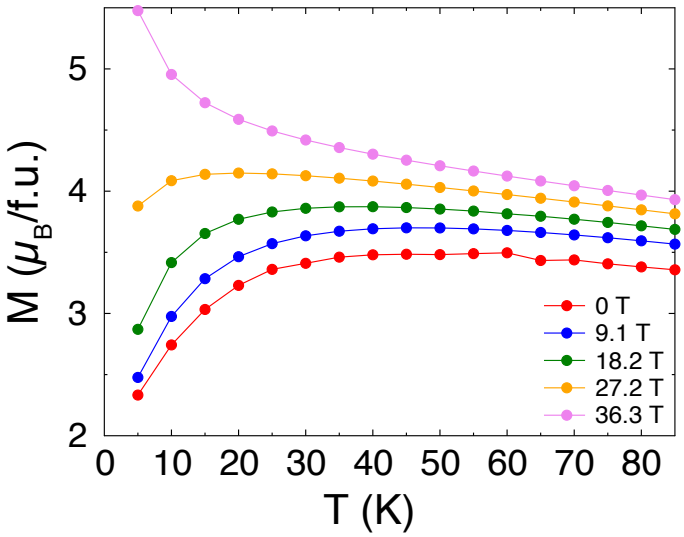

FIG. 9. (color online) Total magnetization as a function of temperature T for different field (different colors) varying from 0 T to 35.3 T.

the moments parallel to each other. Compared to experiment (cf. Fig. 4(b)) the theoretically obtained switching field is by a factor six larger than the experimental one. The discrepancy is caused by multiple contributions that are not considered within the first principle model: *i)* J_{ij} parameters[50] as well as magnetocrystalline anisotropies[51] depend on the temperature of the system; *ii)* our Monte Carlo simulations based on the semiclassical Heisenberg Hamiltonian take into account only the spin degree-of-freedom. To reflect the proper physics, it requires to simulate combined dynamics of orbital moment and spin degree-of-freedom, which serves as separate study in a future implementation. Here in particular, the Zeeman term $gJ * B$ with a modified Landé factor g will be considered in the spin-orbit Hamiltonian, which couples the total moment gJ to the field; *iii)* We did not take crystal field effects into account for the Nd moment, which may be important. Finally, we note that although we approached the phase transition temperature observed in experiment by our theory, a mismatch of ± 10 K $\approx \pm 1$ meV $\approx \pm 20$ T can be observed. Hence, reproducing the exact energy caused by the external magnetic field is beyond the accuracy of our parametrization and numerical method for a weakly coupled moment as that of Nd.

IV. CONCLUSION

In conclusion, with the help of new magnetic measurements in conjunction with extensive first principles electronic structure calculations and simulations based on realistic parameters, we show that there is no second magnetic transition below the ferromagnetic one at about 200 K in well-ordered Nd_2NiMnO_6. The magnetic transition at 200 K is due to the ferromagnetic ordering of the Ni-Mn sublattice arising from ferromagnetic superexchange Ni-O-Mn connectivities, as has been reported earlier. Earlier reports of a second transition at about 100 K, also attributed to a glassy state by some reports in analogy to the case of La_2NiMnO_6, is absent when the anti-site disorder between Ni and Mn are suppressed, leading to a crystallographically well-ordered sample. Thus, it indicates that the magnetic anomaly observed in some of the earlier studies is due to anti-site disorders giving rise to antiferromagnetic superexchange Ni-O-Ni and Mn-O-Mn connectivities within the Ni-Mn sublattice, leading to frustrations within the ferromagnetic system and cannot be attributed to a second magnetic transition. The pronounced magnetic anomaly in terms of the down-turn of the magnetization with a lowering of temperature below 50 K observed in all samples was predominantly explained in the past as an ordering of the Nd sublattice antiferromagnetically coupled to Ni-Mn sublattice. Our results clearly show that there is no long-range magnetic ordering of the Nd sublattice and that this down-turn is a consequence of a ferromagnetic spin coupling between Nd and Ni-Mn sublattice, with the spin-orbit coupling within less than half-filled Nd $4f$ levels making the orbital moment point opposite to the spin moment. Our results also show that the weak ferromagnetic spin coupling between Nd and Ni-Mn sublattice can be overcome by the application of an applied external magnetic field, to make the downturn into an upturn, with the external and the internal fields nearly cancelling each other at about 3 T applied field; this provides us with a quantitative estimate of the internal field experienced by the Nd spins.

V. ACKNOWLEDGEMENT

We thank the Department of Science and Technology, Government of India, for supporting this research. We also acknowledge the support from Swedish Research Council (VR). The experimental work is in parts supported by Indo-U.S. Joint Center for Rational Control

of Functional Oxides under Indo-U.S. Science and Technology Forum. Use of the Advanced Photon Source was supported by the US Department of Energy, Office of Science, under Contract No. DE-AC02-06CH11357. The theory group thank Lars Nordström and Patrik Thunström for fruitful discussions and acknowledges the computational resources provided by the Swedish National Infrastructure for Computing (SNIC). In addition, O.E. acknowledges the support from eSSENCE, STandUPP, the foundation for strategic research (SSF) and the KAW Foundation (Grants No. 2012.0031 and No. 2013.0020). D.D.S. thanks Jamsetji Tata Trust for support.

---

* Present Address: Institute for Methods and Instrumentation in Synchrotron Radiation Research FG-ISRR, Helmholtz-Zentrum Berlin für Materialien und Energie, Albert-Einstein-Strasse 15, 12489 Berlin, Germany

† Also at Jawaharlal Nehru Centre for Advanced Scientific Research, Bengaluru; Email: sarma@iisc.ac.in

[1] K. I. Kobayashi, T. Kimura, H. Sawada, K. Terakura, and Y. Tokura, Nature **395**, 677 EP (1998), URL http://dx.doi.org/10.1038/27167.

[2] D. D. Sarma, P. Mahadevan, T. Saha-Dasgupta, S. Ray, and A. Kumar, Phys. Rev. Lett. **85**, 2549 (2000), URL https://link.aps.org/doi/10.1103/PhysRevLett.85.2549.

[3] H. Das, U. V. Waghmare, T. Saha-Dasgupta, and D. D. Sarma, Phys. Rev. Lett. **100**, 186402 (2008), URL https://link.aps.org/doi/10.1103/PhysRevLett.100.186402.

[4] D. Choudhury, P. Mandal, R. Mathieu, A. Hazarika, S. Rajan, A. Sundaresan, U. V. Waghmare, R. Knut, O. Karis, P. Nordblad, et al., Phys. Rev. Lett. **108**, 127201 (2012), URL https://link.aps.org/doi/10.1103/PhysRevLett.108.127201.

[5] A. Wold, R. J. Arnott, and J. B. Goodenough, Journal of Applied Physics **29**, 387 (1958).

[6] S. Pal, S. Govinda, M. Goyal, S. Mukherjee, B. Pal, R. Saha, A. Sundaresan, S. Jana, O. Karis, J. W. Freeland, et al., Phys. Rev. B **97**, 165137 (2018), URL https://link.aps.org/doi/10.1103/PhysRevB.97.165137.

[7] Y. Guo, L. Shi, S. Zhou, J. Zhao, and W. Liu, Applied Physics Letters **102**, 222401 (2013), URL http://scitation.aip.org/content/aip/journal/apl/102/22/10.1063/1.4808437.

[8] H. Guo, J. Burgess, S. Street, A. Gupta, T. G. Calvarese, and M. A. Subramanian, Applied Physics Letters **89**, 022509 (2006), URL http://scitation.aip.org/content/aip/journal/apl/89/2/10.1063/1.2221894.

[9] K. D. Chandrasekhar, A. K. Das, C. Mitra, and A. Venimadhav, J. Phys.: Condens. Matter **24**, 495901 (2012), URL http://stacks.iop.org/0953-8984/24/i=49/a=495901.

[10] N. S. Rogado, J. Li, A. W. Sleight, and M. A. Subramanian, Advanced Materials **17**, 2225 (2005), URL 10.1002/adma.200500737.

[11] S. Zhao, L. Shi, S. Zhou, J. Zhao, H. Yang, and Y. Guo, J. Appl. Phys. **106**, 123901 (2009), URL http://aip.scitation.org/doi/10.1063/1.3269707.

[12] J. B. Goodenough, A. Wold, R. J. Arnott, and N. Menyuk, Phys. Rev. **124**, 373 (1961), URL http://link.aps.org/doi/10.1103/PhysRev.124.373.

[13] G. Blasse, Journal of Physics and Chemistry of Solids **26**, 1969 (1965), URL http://www.sciencedirect.com/science/article/pii/0022369765902313.

[14] V. L. J. Joly, P. A. Joy, S. K. Date, and C. S. Gopinath, Phys. Rev. B **65**, 184416 (2002), URL http://link.aps.org/doi/10.1103/PhysRevB.65.184416.

[15] C. L. Bull, D. Gleeson, and K. S. Knight, J. Phys.: Condens. Matter **15**, 4927 (2003), URL http://stacks.iop.org/0953-8984/15/i=29/a=304.

[16] M. C. Sánchez, J. García, J. Blasco, G. Subías, and J. Perez-Cacho, Phys. Rev. B **65**, 144409 (2002), URL https://link.aps.org/doi/10.1103/PhysRevB.65.144409.

[17] R. I. Dass, J. Q. Yan, and J. B. Goodenough, Phys. Rev. B **68**, 064415 (2003), URL 10.1103/PhysRevB.68.064415.

[18] R. J. Booth, R. Fillman, H. Whitaker, A. Nag, R. M. Tiwari, K. V. Ramanujachary, J. Gopalakrishnan, and S. E. Lofland, Materials Research Bulletin **44**, 1559 (2009), URL http://www.sciencedirect.com/science/article/pii/S0025540809000609.

[19] Y. H. Chenyang Shi and Z. Hu, J. Phys. D: Appl. Phys. **44**, 245405 (2011), URL 10.1016/j.jallcom.2015.07.136.

[20] W. Z. Yang, X. Q. Liu, H. J. Zhao, Y. Q. Lin, and X. M. Chen, J. Appl. Phys. **112**, 064104 (2012).

[21] R. Yadav and S. Elizabeth, J. Appl. Phys. **117**, 053902 (2015), URL http://scitation.aip.org/content/aip/journal/jap/117/5/10.1063/1.4906989.

[22] J. Sánchez-Benítez, M. J. Martínez-Lope, J. A. Alonso, and J. L. García-Muñoz, Journal of Physics: Condensed Matter **23**, 226001 (2011), URL http://stacks.iop.org/0953-8984/23/i=22/a=226001.

[23] K. Asai, K. Fujiyoshi, N. Nishimori, Y. Satoh, Y. Kobayashi, and M. Mizoguchi, J. Phys. Soc. Jpn. **67**, 4218 (1998).

[24] D. Rubi, C. Frontera, J. Fontcuberta, M. Wojcik, E. Jedryka, and C. Ritter, Phys. Rev. B **70**, 094405 (2004), URL https://link.aps.org/doi/10.1103/PhysRevB.70.094405.

[25] D. Rubi, C. Frontera, J. Nogués, and J. Fontcuberta, Journal of Physics: Condensed Matter **16**, 3173 (2004), URL https://doi.org/10.1088%2F0953-8984%2F16%2F18%2F018.

[26] J. P. Perdew and Y. Wang, Phys. Rev. B **45**, 13244 (1992), URL http://link.aps.org/doi/10.1103/PhysRevB.45.13244.

[27] V. I. Anisimov, F. Aryasetiawan, and A. I. Lichtenstein, J. Phys.: Condens. Matter **9**, 767 (1997), URL http://stacks.iop.org/0953-8984/9/i=4/a=002.

[28] S. Chanda, S. Saha, A. Dutta, and T. P. Sinha, Materials Research Bulletin **62**, 153 (2015), URL http://www.sciencedirect.com/science/article/pii/S0025540814007028.

[29] I. L. M. Locht, Y. O. Kvashnin, D. C. M. Rodrigues, M. Pereiro, A. Bergman, L. Bergqvist, A. I. Lichtenstein, M. I. Katsnelson, A. Delin, A. B. Klautau, et al., Phys. Rev. B **94**, 085137 (2016), URL https://link.aps.org/doi/10.1103/PhysRevB.94.085137.

[30] A. Delin, L. Fast, B. Johansson, J. M. Wills, and O. Eriksson, Phys. Rev. Lett. **79**, 4637 (1997), URL https://link.aps.org/doi/10.1103/PhysRevLett.79.4637.

[31] J. Jensen and A. R. Mackintosh, *Rare Earth Magnetism* (Clarendon Press, Oxford, 1991).

[32] J. M. Wills, M. Alouani, P. Andersson, A. Delin, O. Eriksson, and O. Grechnyev, *Full-Potential Electronic Structure Method* (Springer-Verlag, Berlin, 2010).

[33] A. I. Liechtenstein, M. I. Katsnelson, V. P. Antropov, and V. A. Gubanov, Journal of Magnetism and Magnetic Materials **67**, 65 (1987), URL http://www.sciencedirect.com/science/article/pii/0304885387907219.

[34] M. I. Katsnelson and A. I. Lichtenstein, Phys. Rev. B **61**, 8906 (2000), URL http://link.aps.org/doi/10.1103/PhysRevB.61.8906.

[35] A. Grechnev, I. Di Marco, M. I. Katsnelson, A. I. Lichtenstein, J. Wills, and O. Eriksson, Phys. Rev. B **76**, 035107 (2007), URL https://link.aps.org/doi/10.1103/PhysRevB.76.035107.

[36] M. S. S. Brooks and B. Johansson, Journal of Physics F: Metal Physics **13**, L197 (1983), URL http://stacks.iop.org/0305-4608/13/i=10/a=003.

[37] Y. O. Kvashnin, O. Grånäs, I. Di Marco, M. I. Katsnelson, A. I. Lichtenstein, and O. Eriksson, Phys. Rev. B **91**, 125133 (2015), URL https://link.aps.org/doi/10.1103/PhysRevB.91.125133.

[38] P. Bruno, Phys. Rev. B **52**, 411 (1995), URL http://link.aps.org/doi/10.1103/PhysRevB.52.411.

[39] K. Binder and D. Heermann, *Monte Carlo Simulation in Statistical Physics* , vol. 5 of *An Introduction* (Berlin Heidelberg, 2010), springer-verlag ed., URL //www.springer.com/de/book/9783642031625.

[40] O. Eriksson, A. Bergman, L. Bergqvist, and J. Hellsvik, *Atomistic Spin Dynamics*, Foundations and Applications (Oxford University Press, 2016), URL https://global.oup.com/academic/product/atomistic-spin-dynamics-9780198788669.

[41] S. Nimkar, D. D. Sarma, H. R. Krishnamurthy, and S. Ramasesha, Phys. Rev. B **48**, 7355 (1993), URL https://link.aps.org/doi/10.1103/PhysRevB.48.7355.

[42] D. D. Sarma, O. Strebel, C. T. Simmons, U. Neukirch, G. Kaindl, R. Hoppe, and H. P. Müller, Phys. Rev. B **37**, 9784 (1988), URL https://link.aps.org/doi/10.1103/PhysRevB.37.9784.

[43] S. Ray, A. Kumar, D. D. Sarma, R. Cimino, S. Turchini, S. Zennaro, and N. Zema, Phys. Rev. Lett. **87**, 097204 (2001), URL https://link.aps.org/doi/10.1103/PhysRevLett.87.097204.

[44] F. Nolting, A. Scholl, J. Stöhr, J. W. Seo, J. Fompeyrine, H. Siegwart, J. P. Locquet, S. Anders, J. Lüning, E. E. Fullerton, et al., Nature **405**, 767 EP (2000), URL https://doi.org/10.1038/35015515.

[45] K. V. Shanavas, D. Choudhury, I. Dasgupta, S. M. Sharma, and D. D. Sarma, Phys. Rev. B **81**, 212406 (2010), URL https://link.aps.org/doi/10.1103/PhysRevB.81.212406.

[46] P. A. Kumar, R. Mathieu, P. Nordblad, S. Ray, O. Karis, G. Andersson, and D. D. Sarma, Phys. Rev. X **4**, 011037 (2014), URL https://link.aps.org/doi/10.1103/PhysRevX.4.011037.

[47] A. Szilva, M. Costa, A. Bergman, L. Szunyogh, L. Nordström, and O. Eriksson, Phys. Rev. Lett. **111**, 127204 (2013), URL https://link.aps.org/doi/10.1103/PhysRevLett.111.127204.

[48] Y. O. Kvashnin, R. Cardias, A. Szilva, I. Di Marco, M. I. Katsnelson, A. I. Lichtenstein, L. Nordström, A. B. Klautau, and O. Eriksson, Phys. Rev. Lett. **116**, 217202 (2016), URL

https://link.aps.org/doi/10.1103/PhysRevLett.116.217202.

[49] R. Logemann, A. N. Rudenko, M. I. Katsnelson, and A. Kirilyuk, Journal of Physics: Condensed Matter **29**, 335801 (2017), URL https://doi.org/10.1088%2F1361-648x%2Faa7b00.

[50] D. Böttcher, A. Ernst, and J. Henk, Journal of Magnetism and Magnetic Materials **324**, 610 (2012), URL http://linkinghub.elsevier.com/retrieve/pii/S0304885311006299.

[51] A. Buruzs, Ph.D. thesis, cms.tuwien.ac.at, Wien (2008), URL http://www.cms.tuwien.ac.at/media/pdf/phd-thesis/THESIS.PDF.